ORIGINAL PAPER

Study on microscopic flow mechanism of polymer flooding

Huiying Zhong[1] · Yuanyuan Li[1] · Weidong Zhang[1] · Dan Li[2]

Abstract

Polymer flooding plays an important role in chemical enhanced oil recovery (EOR) methods, and has been widely used in oilfields, particularly Daqing, the largest oilfield in China. However, our understanding of the mechanism of polymer flooding is not very clear. The mechanism of a two-phase micro-flow remains a challenge to researchers, because the structural complexity of a porous medium and the rheological property of a non-Newtonian fluid can increase the difficulty in such research. Computational fluid dynamics provides a numerical simulation method for further investigating the mechanism of polymer flooding at the micro-scale. In this study, OpenFOAM was used to study the two-phase micro-flow of both water and polymer flooding. Based on a micro-physical model of a complex pore structure, the continuity equation, momentum equation, and non-Newtonian fluid constitutive equations of a two-phase flow are established, and the phase equation of the two-phase interface is then developed using the volume of fluid methodology. These equations are solved using the InterFoam solver in OpenFOAM. The saturation, pressure, and velocity distribution characteristics of water and polymer flooding were obtained. The results show that the high viscosity of a polymer solution improves the mobility ratio, inhibits the fingering phenomena, increases the displacement area, and improves the displacement efficiency. The breakthrough time of polymer flooding under a Newtonian rheological property occurs 0.3 s later than that of water flooding, and the displacement pressure drop is higher. When the flow reaches a steady state, the displacement pressure drop of polymer flooding under a Newtonian rheological property is five times that of water flooding, and the displacement efficiency increases by 8–20%. In non-Newtonian fluids with a shear thinning characteristic, where the viscosity of the polymer solution is reduced as compared with polymer flooding under a Newtonian rheological property, polymer flooding under a non-Newtonian rheological property occurs 0.1 s earlier, the displacement pressure drop is reduced by 300 Pa, and the displacement efficiency decreases 4%. These research results will provide a theoretical foundation for a micro-flow mechanism of a two-phase flow in a complex pore structure.

Keywords Polymer flooding · Complex pore model · Two-phase micro-flow · OpenFOAM

Introduction

With the growing demand for energy around the world, oil is playing a major role as the leading source of primary energy (Shahsavari et al. 2014; Rui et al. 2017). Since the Daqing oilfield began experimenting with polymer flooding in 1972, the Jilin, Liaohe, Henan, Shengli, and Xinjiang oilfields have carried out pilot experiments and industry applications (Liu and Chen 1999; Liu et al. 2014; Sheng et al. 2015). Recently, the results of the 30 polymer flooding blocks have shown that polymer flooding has been widely used in the development of oilfields as a significant enhanced oil recovery (EOR) method, which can increase the oil recovery by 10%, and thus polymer flooding has become a key technology for EOR (Wang et al. 2000, 2014). Polymer flooding has also become a common and successful method to enhance the viscous oil in western Canada (Rui et al. 2018). Although the applied scale of polymer flooding is very small in the USA, attention has been focused to the polymer flooding technique. Some researches were conducted to study the formation of water-in-oil microdispersions as a novel mechanism to improve oil recovery with low salinity water flooding in carbonate reservoirs; three different

✉ Huiying Zhong
  zhhy987@126.com

1 Key Laboratory for Enhanced Oil &Gas Recovery of the Ministry of Education, Northeast Petroleum University, Daqing 163318, Heilongjiang, China

2 Daqing Oilfield Company Limited, Exploration and Development Research Institute, Daqing 163712, Heilongjiang, China

concentration brine were employed in experiments and the results showed that low salinity water can cause a greater change in the crude oil composition, then this finding was attributed to the formation of water-in-oil mcrodispersions within the crude oil phase, and this phenomenon can increase the sweep efficiency of the water flooding process (Tetteh et al. 2017). In addition, other countries have conducted pilot tests or large-scale polymer flooding projects (Sheng et al. 2015), such as Argentina (EI Tordillo oilfield), Germany (Bockstedt oilfield), Venezuela (Furrial oilfield), and India (Jhalora oilfield). Along with continuous practice and research, the polymer flooding technique has reached a state of mature industrial application, and has improved oil recovery from 5 to 30% around the world (Wang et al. 2013; Zhu 2015). However, after polymer flooding, oil recovery has only reached 40–50%, and more than half of the crude oil has not been recovered, which illustrates that the understanding of polymer flooding is insufficient, and the mechanism of polymer flooding needs to be further studied, particularly the micro-flow mechanism of a polymer solution, which is helpful for further enhancing the oil recovery of polymer flooding.

In many studies using a porous media micro model to investigate the displacement mechanism on a small scale (Hornbrook et al. 1991; Dong et al. 2005), an image analysis has been used to illustrate the results of the displacement mechanism (Doorwar and Mohanty 2011; Sharma et al. 2012). Furthermore, the network model has been widely used to simulate the displacement performance at a small scale. In these models, complex pore geometries are usually represented using simple shapes (Bakke and Øren 1997; Nordhaug et al. 2003; Békri et al. 2005). For the displacement characteristics of polymer flooding, Liu et al. (2017) studied the effects of the structural parameters of micro-pores on the water flooding performance. Moreover, a network model was also used to investigate the mechanism of microscopic residual oil (Jamaloei et al. 2010; Al-Shalabi and Ghosh 2016). Complex pore and throat structures were represented using simple shapes in a pore network, and these shapes were therefore without the pore network characteristics of real rocks. Because the complex structure and topology of an etched model have overcome the shortcomings of a simple model, these physical models have often been used in experiments on microscopic oil displacement, and these models can reflect the characteristics of a real porous medium. Wang et al. carried out micro-displacement oil experiments of residual oil in dead ends using water, glycerin, and hydrolyzed polyacrylamide (HPAM) fluids (Wang et al. 2000). The results showed that improving the mobility ratio can increase the displacement efficiency. A further experiment was performed in which brine first displaced the oil, and after a breakthrough of the brine at the outlet, polymer solution injection began. The brine was fingered through the oil as expected. The polymer injection led to an enlargement of the fingers normal to the displacement direction. More details of the experiments and results described above were given by Buchgraber et al. (2011). Another important property that can influence displacement efficiency is wettability of the reservoir, this property control the breakthrough of water, oil recovery, residual oil saturation, resistance factor, and residual resistance factor. Comparing with the intermediate-wet systems, Shiran and Skauge (2015) found that the more water-wet systems showed higher resistance and residual resistance factors and no or limited extra oil recovery by polymer flooding. With the development of computer technology, a series of advanced image analysis techniques has become a way to investigate micro-displacement mechanisms on a small scale, such as X-ray, CT scan (Hou 2007; Simjoo et al. 2013; Raeini et al. 2014; Liu et al. 2015), and magnetic resonance imaging (MRI) (Chen et al. 1993; Mitchell et al. 2013) techniques. However, such experiments are quite expensive and time-consuming, and it is difficult to obtain a dynamic view. One approach to overcome these limitations is the application of numerical simulation technique. Recently, the digital rock technology was used to simulate the chemical flooding before EOR pilot test, and the polymer flooding, solvent flooding, and surfactant flooding were simulated at different regimes by the direct hydrodynamics (DHD) simulator (Koroteev et al. 2013). The other approach to overcome these experimental limitations is the application of computational fluid dynamics (CFD), which has been applied to solve the governing equations, such as the finite difference method, finite volume method, and finite element method (Liu 2011). Zhang and Yue (2008) conducted a numerical simulation on the flow characteristics of polymer solutions in a simplified flow model ("T" shape), and the results were compared with the experimental results. They found that high viscoelastic polymer solutions can lead to an increased sweep area, and enhance the displacement capability of residual oil in dead ends and throats. The local pressure drop of a viscoelastic fluid in a shrink flowing channel has been calculated using the finite element method. Zhang et al. (2008) studied the displacement characteristic of residual oil at the throats. The coupled finite volume–immersed boundary method is an effective method to understand viscoelastic fluid flow in porous media; the previous study has showed that pore structures have remarkable impact on the flow behavior of viscoelastic fluid, and the different structures would produce different apparent viscosities of fluid (De et al. 2017). In this study, we just overcame this limitation by showing the results of a generic and flexible tool developed for the treatment of a free surface viscoelastic fluid

flow using the finite volume method and VOF methodology. Furthermore, CFD simulations were conducted using the fluid properties and pore geometry for the micro model experiments conducted by Afsharpoor et al. (2012). In addition, the Lattice-Boltzmann method (LBM) has been used as a CFD method to describe the fluid flow in a porous medium. With the LBM (Li and Novotny 2006; Liu et al. 2016) and the level set method (LSM) (Prodanović and Bryant 2006; Jettestuen et al. 2013), the fluid particles were modeled through a time-dependent distribution moving on a regular lattice, which enabled reproducing a viscous flow in a realistic pore space without an idealization of the pore-space geometry. Capturing the pore scales experimentally is difficult. It is therefore useful to achieve a computational tool that established the exact position and shape of the fluid interfaces in realistic fracture geometries. The OpenFOAM packages are a promising tool for this type of development owing to the fact that it (i) is a free open-source CFD package, (ii) has been widely used and tested for incompressible and compressible flows, laminar and turbulent flows, and multiphase flows, among others, (iii) has an intrinsic advantage of being written in C++ object-oriented language, (iv) has an easy implementation of complicated mathematical and complex physical models, allowing users to build their own codes for specific issues, and (v) in addition to its own mesh generator can also easily import meshes from many popular mesh generator packages (Holmes et al. 2012). The solver InterFoam of FOAM was designed for two or more incompressible, isothermal immiscible fluids. A volume of fluid (VOF) phase fraction–based interface capturing method was implemented. The discretization of the flow governing equations was based on the FVM, and was formulated using a collocated variable arrangement.

To date, studies on polymer flooding at the micro-scale are mainly based on experiments (Sheng et al. 2015; Zhu 2015; Zhong et al. 2017). Theoretical studies mainly concentrate on a simplified physical model, which cannot reflect the flow of a polymer solution in a real porous medium, and such investigations have focused on a single-phase flow problem, with few reports given on a two-phase flow (Zhong et al. 2018). Therefore, this study was based on a micro glass-etched model, and the micro-flow mechanism of a two-phase flow in a complex pore structure model was investigated using the OpenFOAM platform. The effects of water and polymer flooding (Newtonian and non-Newtonian with a constant viscosity and shear-thinning rheological property) on the displacement efficiency were compared. These results showed the displacement mechanism of a polymer solution in a porous medium, and this study will provide a new method and theoretical basis for a further investigation into the mechanism of a two-phase micro-flow.

Mathematical background

Physical model

The micro model can reflect the characteristics of real samples, and therefore, the simulation results are very important.

In this study, we simulated the two-dimensional displacement in micro-models containing an etched-pore pattern allowing a direct observation of pore-scale events with a microscope, and used a glass-etched model to consider the geometric and topological properties of real rocks. In addition, a physical 2D model was established. The simulation processes are shown in Fig. 1.

(1) To consider the memory and computation time of the computer, in this study, we took a portion of the glass-etched model saturated oil. As shown in Fig. 1a, a red area indicates the simulation model.
(2) The red area was digitized. In Fig. 1b, the white part represents solid rock, and the black part represents oil saturated in rock pores.
(3) We used SolidWorks to extract the skeleton of the solid, as shown in Fig. 1c.
(4) SolidWorks was used to generate an STL file. The mesh of the solid part (Fig. 1d) was generated using SolidWorks, which was snappied with the background mesh using the snappyHexMesh solver, and finally the calculation network of numerical simulation was obtained, as shown in Fig. 1e.

The number of cells in the 7 mm × 7 mm blocks was about 440,075, the maximum pore diameter was 1.01 mm in the network model, and the minimal throat diameter was 0.13 mm, as shown in Fig. 1e. The initial oil saturation was 100%, as shown in Fig. 1b; that is, all pores are filled with a black part, the viscosity of the crude oil was 9 mPa s, the density of crude oil was 860 kg/m^3, and the surface tension of two-phase flow was 4.8 mN/m. The boundary conditions of the simulation are shown in Fig. 1e. For the walls, no slip boundaries were used.
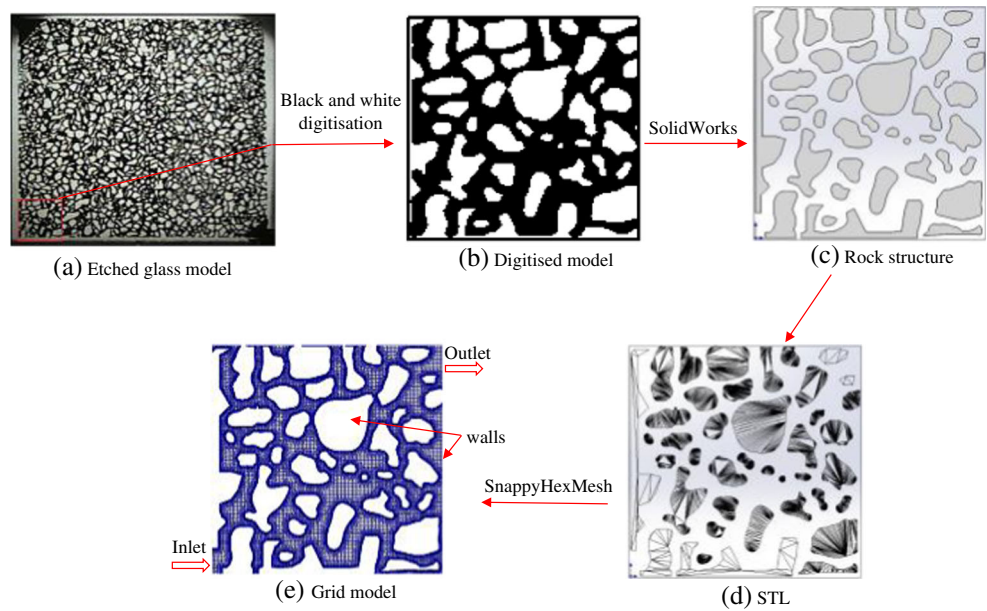
Mathematical model

The flow is isothermal, incompressible, two-dimensional, and immiscible in a complex pore structure. Based on the VOF method, the mathematical model of a two-phase flow was established.

The continuity equation can be written as:

$$\nabla \cdot U_i = 0 \qquad (1)$$

Fig. 1 Micro-pore model and grid partition

(a) Etched glass model   (b) Digitised model   (c) Rock structure

(e) Grid model   (d) STL

where U_i is the velocity vector, m/s; and subscript i denotes the x and y directions, respectively.

The momentum equation is as follows:

$$\frac{\partial \rho U_i}{\partial t} + \nabla \cdot (\rho U_i U_i) - \nabla \cdot \mu \nabla U_i = -\nabla p + F_\sigma \qquad (2)$$

The surface pressure drop F_σ of a two-phase interface through the continuum surface force (CSF) model is as follows (Brackbill et al. 1992; Lafaurie et al. 1994):

$$F_\sigma = \sigma \kappa \nabla \alpha \qquad (3)$$

The formula of curvature κ is

$$\kappa = \nabla \cdot \left(\frac{\nabla \alpha}{|\nabla \alpha|} \right) \qquad (4)$$

where t indicates the time, s; p is the pressure, Pa; ρ is the density of the fluids, kg/m³; μ is the viscosity of the fluids,

Pa s; σ indicates the surface tension coefficient, N/m; κ is the two-phase interface curvature, m⁻¹; and α is the phase volume fraction, which represents the saturation of water.

The polymer solution is a non-Newtonian fluid, and exhibits shear thinning characteristics. The relationship between the viscosity and shear rate of the polymer solution is described using a constitutive equation of the Cross model, in which the viscosity μ is

$$\mu = \mu_\infty + \frac{\mu_0 - \mu_\infty}{1 + (\tau \dot{\gamma})^m} \qquad (5)$$

where μ_0 is the zero shear viscosity, Pa s; μ_∞ is the infinite shear viscosity, Pa s; $\dot{\gamma}$ is the shear rate, s⁻¹; τ indicates the characteristic time, s; and m is the power law index of the Cross model, which is dimensionless. In this study, $\tau = 1$ and $m = 0.5$.

With VOF, α is the phase volume fraction, which is defined as follows:

$$\alpha = \begin{cases} 1 & \text{for a point inside the polymer or water solution} \\ 0 < \alpha < 1 & \text{for a point in the transitional region} \\ 0 & \text{for a point completely in the oil} \end{cases} \qquad (6)$$

Basis on the definition of α and the continuity equation, the phase equation can be expressed as:

$$\frac{\partial \alpha}{\partial t} + \nabla \cdot \alpha U_i = 0 \qquad (7)$$

The local density ρ and viscosity μ of the fluid are

$$\rho = \alpha \rho_0 + (1 - \alpha) \rho_1 \qquad (8)$$

$$\mu = \alpha \mu_0 + (1 - \alpha) \mu_1 \qquad (9)$$

where the subscripts 0 and 1 denote the oil and water or polymer solution.

In this paper, the governing equations consist of Eqs. (1), (2), (5), and (7), and in the OpenFOAM platform, the governing equations were solved using the InterFoam two-phase flow solver.

Numerical simulation results and analysis

In this paper, three schemes were simulated: water displacing oil, a polymer solution displacing oil (Newtonian rheology), and a polymer solution displacing oil (non-Newtonian rheology). Table 1 lists the parameters used. In all simulations, the mass flow at the inlet liquid rate was 2.5×10^{-9} m^3 s, and the outlet pressure was fixed at 0 Pa. Using the post processing ParaView solver of the OpenFOAM platform, the saturation, velocity, and pressure distribution at different times can be obtained.

Water displacing oil

At 0.8 s, the CFD simulation results for water displacing oil are shown in Fig. 2, where alpha refers to the water saturation. The middle diagram shows the velocity distribution in the micro model. In addition, the third diagram shows the pressure distribution.

As can be seen in Fig. 2, (a) shows the position of the yellow circle indicates severe fingering after the water enters the complex pores, (b) shows the velocity in the complex pores, where the greatest flow velocities correspond with the fingers, and (c) shows the pressure distribution. A high pressure is at the inlet, a low pressure is at the outlet, and a dead end with a poor connectivity forms a local high-pressure area. After oil with large pores is displaced, the prevailing pores are formed. Therefore, low viscosity fluid (water) enters the flow paths leading to a further growth of the fingers, and the fingering phenomenon results in poor displacement efficiency of the water.

Polymer displacing oil (Newtonian rheological property)

At 0.8 s, the CFD simulation results of a polymer solution (Newtonian rheological property) are as shown in Fig. 3. Because Newtonian fluids do not have shear thinning characteristics, the viscosity of the polymer solution was constant.

Compared with water flooding, the polymer flooding under a Newtonian rheological property has a small fingering. As illustrated in Fig. 3a, the position of the yellow circle indicates slight fingering. In the pores, water flooding has a smaller velocity than polymer flooding, increasing the sweep area, and polymer flooding cannot form prevailing pores. In addition, the high viscosity of polymer flooding increases the displacement pressure, improving the displacement efficiency. At a dead end, a local high-pressure polymer flooding (Newtonian rheological property) is formed, and the pressure is higher than in water flooding.

Polymer displacing oil (non-Newtonian rheological property)

At 0.8 s, the CFD simulation results for polymer displacing oil (non-Newtonian rheological property) are demonstrated in Fig. 4. Under a non-Newtonian rheological property, the polymer solution exhibits a shear thinning characteristic, a larger shear rate for the polymer solution, and a lower viscosity.

As can be seen from Fig. 4a, the yellow circle indicates the occurrence of severe fingering. The fingering phenomenon is slower than in water flooding, but is more obvious than in polymer flooding under a Newtonian rheological property. In a flowing channel, polymer flooding under a non-Newtonian rheological property has a lower velocity than water flooding, whose sweep area is poorer than polymer flooding (Newtonian rheological property), and cannot form a prevailing pore. At the dead ends, the polymer solution of a non-Newtonian fluid forms a local high pressure, which occurs between the water flooding and polymer flooding (Newtonian rheological property).

To compare the breakthrough time of the three simulated schemes, the saturation in the outlet flow time diagram

Table 1 Parameters of two-phase flow

| Scheme	Oil		Displacement fluid		Two-phase area
	Density (kg/m^3)	Viscosity (mPa s)	Density (kg/m^3)	Viscosity (mPa s)	Interfacial tension (mN/m)
Water flooding	860	9	1000	1	4.8
Polymer flooding (Newtonian rheology)	860	9	1000	9	4.8
Polymer flooding (Non-Newtonian rheology)	860	9	1000	9	4.8

Fig. 2 CFD simulation results for water ($\mu = 1$ mPa s) displacing oil ($\mu_o = 9$ mPa s) (**a** presenting the saturation distribution, the water is represented in blue and the oil in red, and the area enclosed by yellow circle shows the finger breakthrough intuitively; **b** presenting the velocity distribution, and the velocity is great in the main flow-path; **c** is the pressure distribution in porous media, the pressure is high in inlet and is low in outlet, and the dead oil can be easily formed in the higher pressure area)

(a) Alpha (saturation)

(b) Velocity magnitude (m/s)

(c) Pressure (Pa)
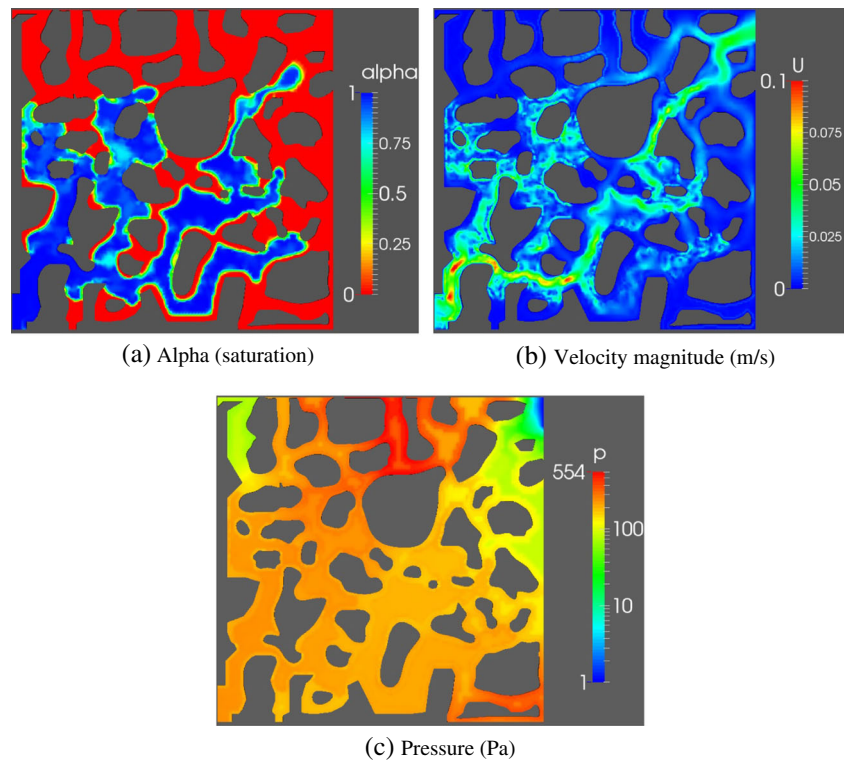
according to the simulation results of the CFD is shown in Fig. 5. Before a breakthrough occurs, alpha (α) is fixed at zero, which illustrates that the fluid produced at the outlet is only oil. The value of alpha (α) increases after a breakthrough,

thereby indicating that the fluids produced are oil and water, and with an increase in alpha (α), the water cut increases as well. At 1 s, the water flooding front incurs a breakthrough, after which the saturation curves show a jumpy fluctuation,

Fig. 3 CFD simulation results for polymer (Newtonian rheology) ($\mu = 9$ mPa s) displacing oil ($\mu_o = 9$ mPa·s) (**a** showing the saturation distribution, the water is represented in blue and the oil in red, and the front velocity is almost the same; **b** showing the velocity distribution, and the velocity is great in the main flow-path and in the throat; **c** is the pressure distribution in porous media, and the pressure is high in inlet and is low in outlet)

(a) Alpha (saturation)

(b) Velocity magnitude(m/s)

(c) Pressure(Pa)
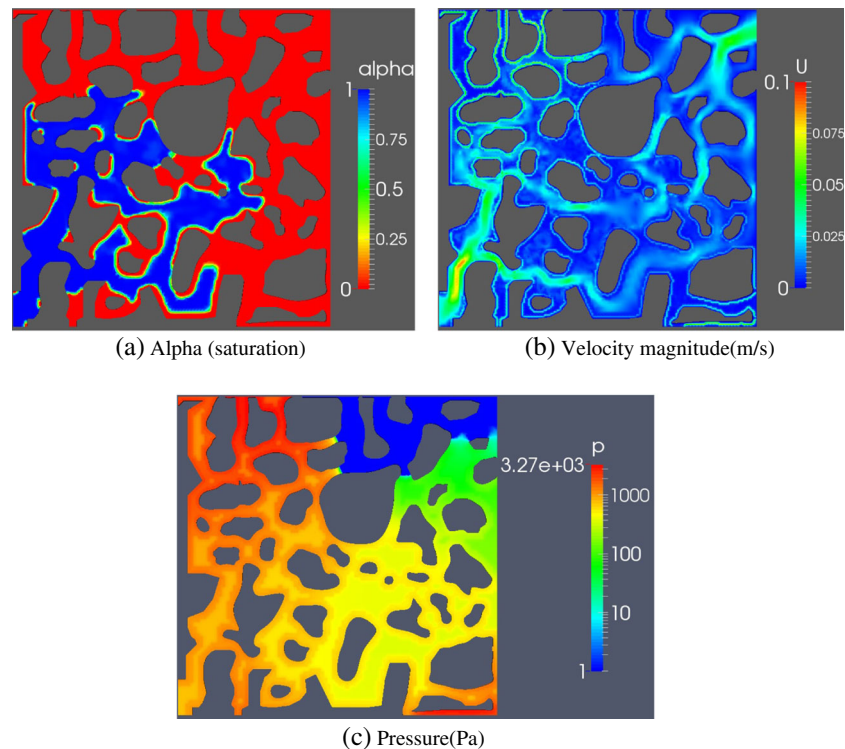
Fig. 4 CFD simulations results for polymer (non-Newtonian rheology) ($\mu = 9$ mPa s) displacing oil ($\mu_o = 9$ mPa s) (**a** showing the saturation distribution, the water is represented in blue and the oil in red; **b** showing the velocity distribution, and the velocity is great in the main flow-path; **c** is the pressure distribution in porous media, and the pressure is high in inlet and is low in outlet)

(a) Alpha (saturation)


(b) Velocity magnitude(m/s)

(c) Pressure(Pa)
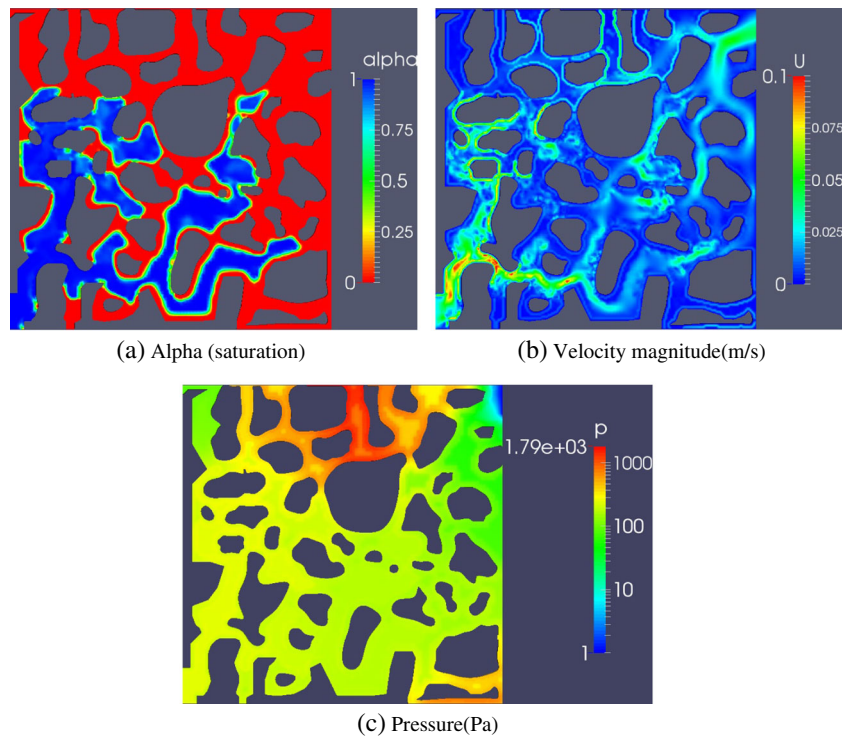
which indicates that the water flooding efficiency does not stabilize. Compared with water flooding, the displacement front of the polymer flooding under a Newtonian rheology breakthrough occurs 0.3 s later than that of water flooding, and the displacement front of polymer flooding under a non-Newtonian rheology breakthrough occurs 0.2 s later than that of water flooding. For a polymer solution under a non-Newtonian rheological property, the breakthrough time occurs 0.1 s earlier than in polymer flooding under a Newtonian rheological property. However, for polymer flooding, the value of the saturation alpha (α) is slightly increased, and the displacement efficiency is stabilized. Moreover, we can conclude that the variation of shear rate is the same with that of velocity in the throat by an analysis of Figs.4 and 5, and the shear rate is higher than that in the pore. It should be noted that

the shear rate in the wall of pore sometimes is higher than that in the center of pore. This is in agreement with the existing knowledge that the shear rate is not only related to the flow velocity but also the position, and hence parameters like local pore geometry (Berg and van Wunnik 2017).

The displacement pressure drop relationship between the inlet and outlet is shown in Fig. 6. For water flooding, the pressure drop of the inlet and outlet rapidly declines. After 1 s, the pressure drop curve stabilizes. Compared with water flooding, during the entire displacement process, the pressure drop of polymer flooding under a Newtonian rheological property is higher than that in water flooding, and not only does the pressure drop curve show a slow decline, the amount of the pressure drop is also small. After a breakthrough, the stable pressure drop is five times that of water flooding. For

Fig. 5 Saturation at outlet vs. time
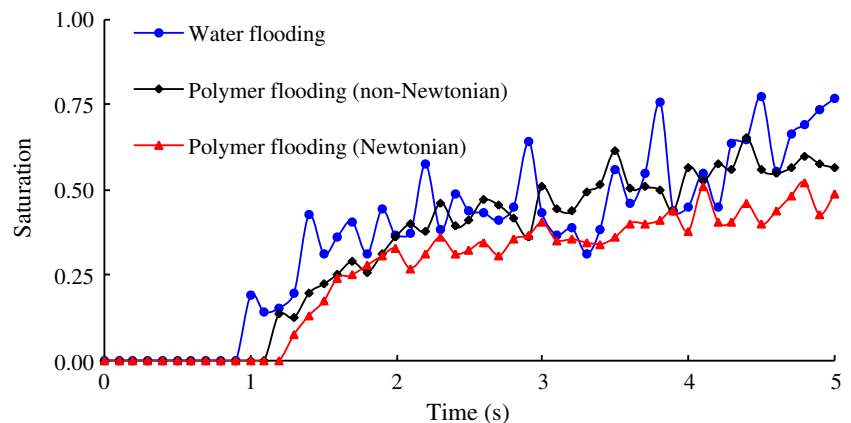
Fig. 6 Pressure drop between inlet and outlet vs. time
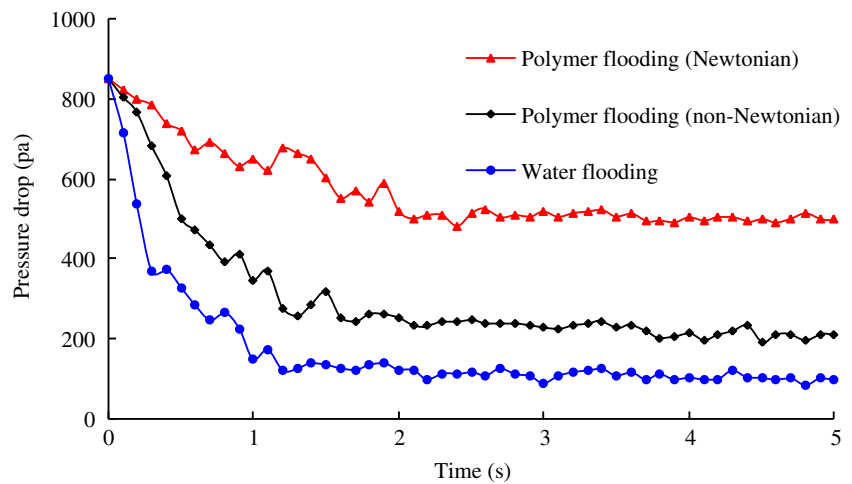
polymer flooding under a non-Newtonian rheological property, the pressure drop of the displacement is higher than in water flooding, and after stabilization, pressure drop is twice that of water flooding.

For a qualitative analysis, in this study, the area method was used to calculate the displacement efficiency under different displacement processes and displacement fluids. The displacement efficiency is defined as

$$\eta = \frac{A_0 - A_{red}}{A_0} \times 100\% \tag{10}$$

where η is the displacement efficiency; A_0 is the initial oil area of the entire complex pore area, m^2; and A_{red} is the residual oil area, as indicated by the red section in the saturation distribution figure, m^2.

The displacement efficiency is shown in Fig. 7. Before a water flooding breakthrough, the three schemes show the same displacement efficiency, which increases with the linear properties. After a breakthrough, the curve of the water flooding is slightly increased owing to the later breakthrough in polymer flooding than in water flooding, and the displacement efficiency is still increased. For non-Newtonian fluids, the shear thinning of the polymer solution decreases the viscosity and the breakthrough occurs earlier. The displacement efficiency is lower than the constant viscosity of polymer flooding. At a breakthrough, the displacement efficiency of polymer flooding under a non-Newtonian rheological property is 8% higher than that of water flooding, and the polymer flooding under a Newtonian rheological property is 4% higher than the polymer flooding under a non-Newtonian rheological property. After a breakthrough, compared with water flooding process, both the displacement efficiency with Newtonian polymer flooding and the displacement efficiency with non-Newtonian polymer flooding increase 8–20% at different times.

Fig. 7 Displacement efficiency of water and polymer flooding
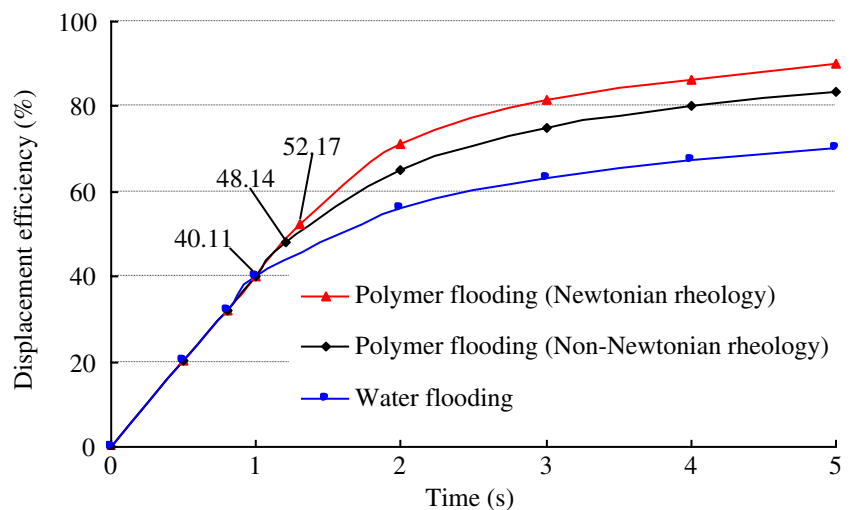
Conclusions

(1) Based on the glass-etched model, a complex pore network model of a porous medium is established, which has the geometric and topological properties of real rock. CFD simulations show the displacement processes of real rocks, increasing the realism and reliability of the simulation.

(2) The high viscosity of a polymer solution improves the mobility ratio, decreases the velocity of the displacement front, and inhibits the fingering phenomenon; in addition, the breakthrough time is 0.2–0.3 s longer than in water flooding. In a flowing channel, the velocity of polymer flooding is slower than that of water flooding, which increases the sweep area and prohibits the formation of prevailing pores. A polymer solution can increase the pressure drop, thereby increasing the displacement efficiency.

(3) After a breakthrough, the water cut in water flooding rises rapidly, whereas the water cut in polymer flooding increases slightly. During the displacement process, the displacement efficiency of polymer flooding is 8–20% higher than that of water flooding.

(4) Owing to the shear thinning characteristic of non-Newtonian fluids, the viscosity of a polymer solution is reduced, the mobility ratio of the displacement processes is increased, and the displacement efficiency is decreased. Compared with the polymer flooding under a Newtonian rheological property, the displacement efficiency decreases by ∼4%.

References

Afsharpoor A, Balhoff MT, Bonnecaze R, Huh C (2012) CFD modeling of the effect of polymer elasticity on residual oil saturation at the pore-scale. J Pet Sci Eng 94-95:79–88

Al-Shalabi EW, Ghosh B (2016) Effect of pore-scale heterogeneity and capillary-viscous fingering on commingled waterflood oil recovery in stratified porous media. J Petrol Eng 2016:1708929

Bakke S, Øren PE (1997) 3-D pore-scale modelling of sandstones and flow simulations in the pore networks. SPE J 2(2):136–149

Békri S, Laroche C, Vizika O (2005) Pore network models to calculate transport and electrical properties of single or dual-porosity rocks. In: SCA2005–35, Proceedings of the International Symposium of the Society of Core Analysts, Toronto, Canada

Berg S, van Wunnik J (2017) Shear rate determination from pore-scale flow fields. Transport Porous Med 117(2):229–246

Brackbill JU, Kothe DB, Zemach C (1992) A continuum method for modelling surface tension. J Comput Phys 100(2):335–354

Buchgraber M, Clemens T, Castanier LM, Kovscek A (2011) A microvisual study of the displacement of viscous oil by polymer solutions. SPE Reserv Eval Eng 14(3):269–280

Chen S, Qin F, Kim K-H, Watson AT (1993) NMR imaging of multiphase flow in porous media. AICHE J 39(6):925–934

De S, Kuipers JAM, Peters EAJF, Padding JT (2017) Viscoelastic flow simulations in random porous media. J Non-Newton Fluid 248:50–61

Dong M, Foraie J, Huang S, Chatzis I (2005) Analysis of immiscible water-alternating-gas (WAG) injection using micromodel tests. J Can Pet Technol 44(2):17–25

Doorwar S, Mohanty KK (2011) Viscous fingering during non-thermal heavy oil recovery. In: SPE-146841-MS, Proceedings of the SPE Annual Technical Conference and Exhibition, Denver, Colorado, USA

Holmes LT, Favero J, Osswald T (2012) Numerical simulation of three-dimensional viscoelastic planar contraction flow using the software OpenFOAM. Comput Chem Eng 37:64–73

Hornbrook JW, Castanier LM, Pettit PA (1991) Observation of foam/oil interactions in a new, high-resolution micromodel. In: SPE-22631-MS, Proceedings of the SPE Annual Technical Conference and Exhibition, Dallas, Texas, USA

Hou J (2007) Network modeling of residual oil displacement after polymer flooding. J Pet Sci Eng 59(3–4):321–332

Jamaloei BY, Asghari K, Kharrat R, Ahmadloo F (2010) Pore-scale two-phase filtration in imbibition process through porous media at high- and low-interfacial tension flow conditions. J Pet Sci Eng 72(3–4):251–269

Jettestuen E, Helland JO, Prodanović M (2013) A level set method for simulating capillary-controlled displacements at the pore scale with nonzero contact angles. Water Resour Res 49(8):4645–4661

Koroteev DA, Dinariev O, Evseev N, Klemin DV, Safonov S, Gurpinar OM, Berg S, van Kruijsdijk C, Myers M, Hathon L, de Jong H, Armstrong R (2013) Application of digital rock technology for chemical EOR screening. In: SPE-165258-MS, Proceedings of the SPE Enhanced Oil Recovery Conference, Kuala Lumpur, Malaysia

Lafaurie B, Nardone C, Scardovelli R, Zanetti G, Zaleski S (1994) Modeling merging and fragmentation in multiphase flows with SURFER. J Comput Phys 113(1):134–147

Li X, Novotny RJ (2006) Study on cement displacement by Lattice-Boltzmann method. In: SPE-102979-MS, Proceedings of the SPE Annual Technical Conference and Exhibition, San Antonio, Texas, USA

Liu Y (2011) Exact solutions to nonlinear Schrödinger equation with variable coefficients. Appl Math Comput 217(12):5866–5869

Liu Y, Chen G (1999) Optimal parameters design of oilfield surface pipeline systems using fuzzy models. Inf Sci 120(1):13–21

Liu Y, Wang Z, Zhuge X, Pang R (2014) Distribution of sulfide in an oil-water treatment system and a field test of treatment technology in Daqing oilfield. Pet Sci Technol 32(4):462–469

Liu Y, Li JX, Wang Z, Wang S, Dong Y (2015) The role of surface and subsurface integration in the development of a high-pressure and low-production gas field. Environ Earth Sci 73:5891–5904

Liu H, Kang Q, Leonardi CR, Schmieschek S, Narváez A, Jones BD, Williams JR, Valocchi AJ, Harting J (2016) Multiphase lattice Boltzmann simulations for porous media applications. Comput Geosci 20(4):777–805

Liu Z, Yang Y, Yao J, Zhang Q, Ma J, Qian Q (2017) Pore-scale remaining oil distribution under different pore volume water injection based on CT technology. Adv Geo-energ Res 1(3):171–181

Mitchell J, Chandrasekera TC, Holland DJ, Gladden LF, Fordham EJ (2013) Magnetic resonance imaging in laboratory petrophysical core analysis. Phys Rep 526(3):165–225

Nordhaug HF, Celia M, Dahle HK (2003) A pore network model for calculation of interfacial velocities. Adv Water Resour 26(10):1061–1074

Prodanović M, Bryant SL (2006) A level set method for determining critical curvatures for drainage and imbibition. J Colloid Interface Sci 304(2):442–458

Raeini AQ, Blunt MJ, Bijeljic B (2014) Direct simulations of two-phase flow on micro-CT images of porous media and upscaling of pore-scale forces. Adv Water Resour 74:116–126

Rui Z, Peng F, Ling K, Chang H, Chen G, Zhou X (2017) Investigation into the performance of oil and gas projects. J Nat Gas Sci Eng 38: 12–20

Rui Z, Wang X, Zhang Z, Lu J, Chen G, Zhou X, Patil S (2018) A realistic and integrated model for evaluating oil sands development with steam assisted gravity drainage technology in Canada. Appl Energy 213:76–91

Shahsavari AA, Khodaei K, Hatefi R, Asadian F, Zamanzadeh SM (2014) Distribution of total petroleum hydrocarbons in Dezful aquifer, Southwest of Iran. Arab J Geosci 7(6):2367–2375

Sharma J, Inwood SB, Kovscek A (2012) Experiments and analysis of multiscale viscous fingering during forced imbibition. SPE J 17(4): 1142–1159

Sheng JJ, Leonhardt B, Azri N (2015) Status of polymer-flooding technology. J Can Pet Technol 54(2):116–126

Shiran BS, Skauge A (2015) Wettability and oil recovery by polymer and polymer particles. In: SPE-174568-MS, Proceedings of the SPE Asia Pacific Enhanced Oil Recovery Conference, Kuala Lumpur, Malaysia

Simjoo M, Dong Y, Andrianov A, Talanana M, Zitha PLJ (2013) CT scan study of immiscible foam flow in porous media for enhancing oil recovery. Ind Eng Chem Res 52(18):6221–6233

Tetteh JT, Rankey E, Barati R (2017) Low salinity waterflooding effect: Crude oil/brine interactions as a recovery mechanism in carbonate rocks. In: OTC-28023-MS, Proceedings of the Offshore Technology Conference Brasil, Rio de Janeiro, Brazil

Wang D, Cheng J, Yang Q, Guo W, Li Q, Chen F (2000) Visco-elastic polymer can increase microscale displacement efficiency in cores. In: SPE-63227-MS, Proceedings of the SPE Annual Technical Conference and Exhibition, Dallas, USA

Wang Z, Le X, Feng Y, Zhang C (2013) The role of matching relationship between polymer injection parameters and reservoirs in enhanced oil recovery. J Pet Sci Eng 111:139–143

Wang Z, Liu Y, Le X, Yu H (2014) The effects and control of viscosity loss of polymer solution compounded by produced water in oilfield development. Int J Oil Gas Coal Technol 7(3):298–307

Zhang L, Yue X (2008) Displacement of polymer solution on residual oil trapped in dead ends. J Cent S Univ Technol 15(Suppl 1):84–87

Zhang L, Yue X, Guo F (2008) Micro-mechanisms of residual oil mobilization by viscoealstic fluids. Pet Sci 5(1):56–61

Zhong H, Zhang W, Yin H, Liu H (2017) Study on mechanism of visco-elastic polymer transient flow in porous media. Geofluids 2017: 8763951

Zhong H, Li Y, Zhang W, Yin H, Lu J, Guo D (2018) Microflow mechanism of oil displacement by viscoelastic hydrophobically associating water-soluble polymers in enhanced oil recovery. Polymers 10(6):628

Zhu Y (2015) Current developments and remaining challenges of chemical flooding EOR techniques in China. In: SPE-174566-MS, Proceedings of the SPE Enhanced Oil Recovery Conference, Kuala Lumpur, Malaysia